Tribology International 160 (2021) 107020

Contents lists available at ScienceDirect

Tribology International

journal homepage: http://www.elsevier.com/locate/triboint

Reduced sliding friction on flat and microstructured metal injection molded (MIM) WC-Co hard metals with MoS_2 composite lubricants

Christopher K. Dawari [a], Inzimam Haq [a], Kari Mönkkönen [b], Mika Suvanto [a], Jarkko J. Saarinen [a,*]

[a] Department of Chemistry, University of Eastern Finland, P.O. Box 111, FI-80101 Joensuu, Finland
[b] Karelia University of Applied Sciences, FI-80200 Joensuu, Finland

ARTICLE INFO

Keywords:
Dynamic coefficient of friction (COF)
Lubricating grease
Solid lubricants
MoS_2
Reciprocating sliding friction
Pin-on-plate

ABSTRACT

Surface texturing with lubricant mixtures was studied by dynamic coefficient of friction (COF) values on micropit and micropillar WC-Co hard metal specimens that were fabricated using a micro-working robot technique combined with metal injection molding (MIM). Lubricating grease mixed with MoS_2 was investigated, and 40 wt % additive level of MoS_2 reduced COF values by 45% down to 0.06 level on flat WC-Co specimens. The corresponding COF values for the micropit specimens were higher up to 0.10 that may result from the small contact area of the used pin. On the contrary, a reduction of COF values was observed for micropillar specimens compared to the flat WC-Co specimens induced by a load carrying structure of the micropillar specimen. A highly stable antiwear behavior was observed for specimens with micropits.

1. Introduction

Layered crystallites, commonly known as solid lubricants, have been extensively used as additives in oils [1,2] and greases [3] for reducing friction and wear in mobile mechanical assemblies. They can be used directly as powders, fillers in self lubricating composites and as additives to liquid lubricants. Good lubricity is due to weak van der Waals forces between the planar sheets which allows easy shearing between the basal layers. Their operation, however, is highly dependent on environmental factors such as atmosphere, humidity and radiation. Typical examples of layered solids are graphite, transition metal dichalcholgenides (for example, MoS_2 [4] and WS_2 [5]) and hexagonal boron nitride (h-BN) [6,7] from which MoS_2 is probably the most studied and widely utilized [8].

MoS_2 occurs naturally as a black crystallite that is obtained as molybdenite, a mineral ore of molybdenum. It can also be fabricated synthetically. An extensive review of the basic structure, synthesis, application and lubricating mechanisms of MoS_2 can be found from a previous study [9]. The basic mechanisms of the lubricating properties of MoS_2 is the ability to form a transfer film on a counter surface, and the shear orientation of the basal planes along the sliding direction [9,10]. Reliable operation window covers a wide temperature range from cryogenic temperatures to about 300 °C in air. In addition, ability to operate effectively also in vacuum allows MoS_2 lubricant for a wide range of applications including space industry. It has also been used in several tribological applications on different substrates from stainless steel [11] and ceramic materials to hard metals [12] and polymers [13]. MoS_2 can be applied onto surfaces of mechanical components, for example, by rubbing (burnishing) on textured cemented carbide [14], titanium alloys [15] and steel surfaces [16], spraying [17] and hot pressing [18]. It can also be deposited as surface coating material by magnetron sputtering [19] or mixed together with lubricants ranging from low viscosity oils [20] and engine oil [21] to liquid paraffin [22].

Over the recent years, surface texturing has been studied as a surface pretreatment method with solid lubricants. A focused review of common surface texturing techniques that have been tested and used in the past decades was presented in a previous study [23]. A more recent surface texturing technique is the combination of a computer controlled micro-working robot technique with metal injection molding (MIM) [24]. MIM is useful technique in fabricating highly precise, controlled micropillars, micropits and multilevel micropits on metal surfaces including also ceramic materials [24]. Micro-dimple structure by infrared [25], laser [26], and electrochemical [27] surface texturing has been reported in literature as a particularly promising method for reducing friction and wear between rubbing surfaces in hydrodynamic, hydrostatic and mixed lubrication regimes as they serve as reservoires

* Corresponding author.
E-mail address: jarkko.j.saarinen@uef.fi (J.J. Saarinen).

https://doi.org/10.1016/j.triboint.2021.107020
Received 15 December 2020; Received in revised form 10 March 2021; Accepted 23 March 2021
Available online 26 March 2021

for lubricants and also as wear debris entrapment cavities. Texturing can also enhance the load carrying capacity of mechanical components [28] and also increase hydrodynamic pressure effect in a lubricated contact [29].

In this study the effect of a mixed lubricant of MoS_2 and lubricating grease on the sliding friction and wear properties was studied on both on flat and textured WC-Co hard metal specimens. Highly controlled micropit and micropillar WC-Co specimens were fabricated using MIM with needle sizes of 100 μm and 200 μm. Sliding friction was measured using pin-on-plate reciprocating sliding tests on tribometer with two normal loads of 10 N and 30 N. First, the additive levels of MoS_2 were examined on flat reference specimens for a low friction surfaces. Secondly, the effect of both micropit and micropillar density was studied with the hihg density micropillars displayeing the lowest COF values. The observed sliding friction results were complemented with detailed surface morphology characterization by using the scanning electron microscope (SEM).

2. Materials and methods

2.1. Sample preparation

Fig. 1 shows the fabrication protocol of the WC-Co micropit specimens. First, highly ordered round shaped micropits were fabricated on a rectangular (64 mm × 1 mm) 0.25 mm thick nickel foil (99.99%, Good Fellow Cambridge Limited, UK) using a computer assisted laboratory scale micro-working robot (Mitsubishi rp-1ah robot 1). Nickel foils were textured at a speed of 500 mm/s. Micropits were created using two WC-Co needles (Fodesco Ltd, FI) with tip diameters of 100 μm and 200 μm. High density, medium density and low density micropit arrays were created using the 200 μm needle assembled to the arm of the microbot. The separation between adjacent pit locations for each array was 200 μm, 400 μm and 600 μm, respectively. The 100 μm needle was used to create micropits with a separation of 100 μm between adjacent pit locations. Micropits were ordered in an equidistant square lattice arrangement on each matrix.

Secondly, to fabricate ordered hard metal WC-Co micropit specimens, each micropit matrix on Ni foil was replicated on 17-4PH stainless steel (PolyMIM GmbH, DE; composition shown in Table 1) having micropillars. The 17-4PH micropillar sample was then used as a mold insert to fabricate WC-CO hard metal micropit samples, and 17-4PH was selected as a mold material due to a low coefficient of expansion during sintering.

Table 1
Typical composition of commercially graded 17-4PH stainless steel specimens.

Composition	Fe	C	Ni	Cr	Mn	Si	Cu	other
>	–	–	3.0	15.0	–	–	3.0	–
<	Balance	0.07	5.0	17.5	1.0	1.0	5.0	0.45

Finally, the micropillar WC-Co specimens were fabricated in a single MIM replication process using Ni mold inserts with 200 μm and 400 μm separation between the adjacent micropit locations in a square lattice produced with the microrobot. The micropillar WC-Co specimens (a negative of the micropit texture on the Ni mold inserts) were then replicated using a MIM process similar to the 17-4PH SS specimens.

Each fabrication and replication process was carried out by MIM technique using a HAAKE Minijet II (Thermo Fisher Scientific) injection molding micro-compounder under the following parameters: cylinder temperature of 191 °C, heating tool temperature of 60 °C, injection pressure of 750 bar and injection time of 10 s. These specimens, technically referred to as the green parts, with an average thickness of 1.64 mm were debinded, dried and sintered. The polymer binder material was removed from the compounded green parts by solvent debinding by placing the specimens into a hot water bath at a constant temperature of 60 °C for 12 h. These so called brown parts were subsequently dried in a temperature programmed oven at temperature of 100 °C for 2 h. Full densification of specimens was achieved through a liquid phase sintering protocol in a high temperature furnace (HTK 8 MO/16-1G, Carbolite/Gero, DE).

For the 17-4PH insert specimens, sintering was carried out in an H_2 atmosphere with the following successive sintering protocol as presented in Fig. 2 A: heating from room temperature to 200 °C at a heating rate of 180 °C /h for 1 h (A) and holding for 2 h, heating from 200 °C to 600 °C at 180 °C /h for 2 h 13 min (B) and holding for 2 h, heating from 600 °C to 1 350 °C at 300 °C/h for 2 h 30 min (C) and holding for 3 h followed by cooling from 1 350–80 °C for 1 h 25 min at 900 °C /h (D) and holding for 15 min before cooling from 80 °C to room temperature.

The sintered 17-4PH specimens were utilized as new mold inserts to fabricate WC-Co specimens with micropits arrayed in an exact negative compared to the micropillars of mold inserts. The main feedstock material for MIM micropit specimens was commercial cemented tungsten carbide, (WC-Co, WC0.8Co13.5, Z360, PolyMIM GmbH, DE). The feedstock had an average density of 14 g/cm^3 and a Vicker hardness greater than 1440 HV_{10}. The composition of the feedstock material is presented in Table 2. Both micropillar and micropit MIM specimens

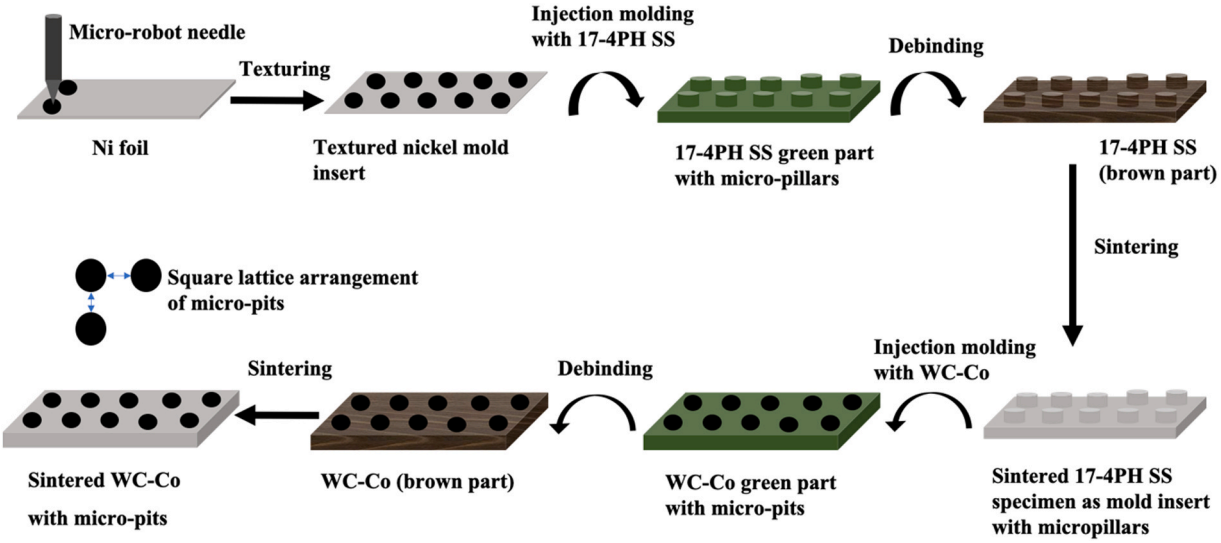

Fig. 1. Fabrication of WC-Co micropit specimens by micro-robot and MIM techniques.

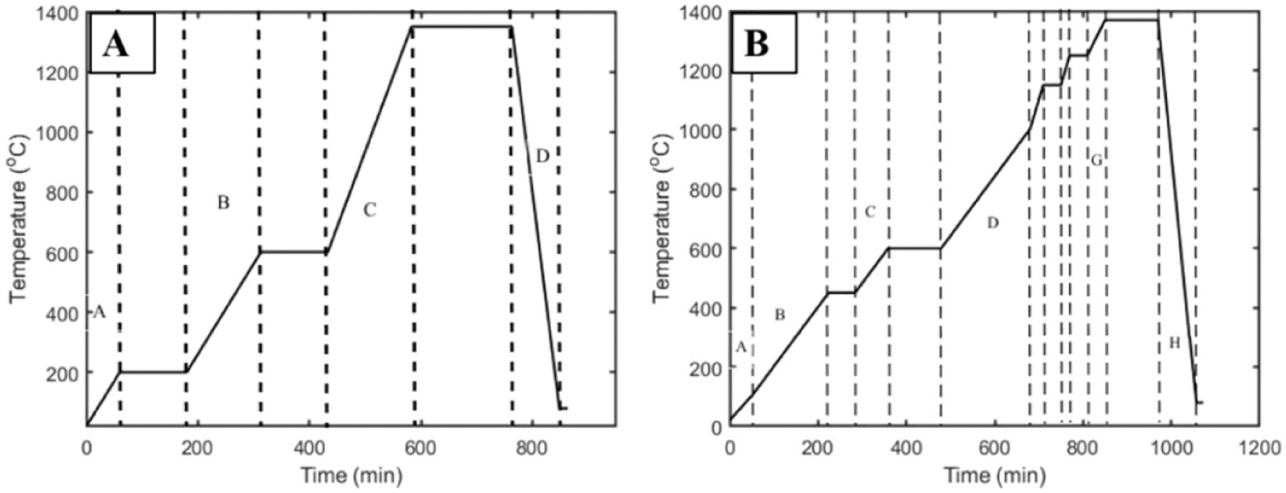

Fig. 2. Sintering protocols for; (A) 17-4PH SS and (B) WC-Co specimens.

Table 2
Typical composition of commercially graded WC-Co.

Composition	WC	Co	Other carbides
>	–	13.0	–
<	Balance	14.0	0.7

were produced using HAAKE Minijet II injection molding device.

The WC-Co green parts were debinded and dried as given above. The debinded brown WC-Co samples were sintered in an N_2 atmosphere with the following protocol as presented in Fig. 2 B: heating from room temperature to 100 °C at 100 °C/h for 48 min (A) and holding for 1 min, heating from 100 °C to 450 °C at 120 °C/h for 2 h 55 min (B) and holding for 1 h, heating from 450 °C to 600 °C at 120 °C/h for 1 h 15 min (C) and holding for 2 h, heating from 600 °C to 1 000 °C at 120 °C/h for 3 h 20 min (D) and holding for 1 min, heating from 1 000 °C to 1 150 °C at 300 °C/h for 30 min (E) and holding for 40 min, heating from 1 150 °C to 1 250 °C at 300 °C/h for 20 min (F) and holding for 40 min, heating from 1 250 °C to 1 369 °C at 180 °C/h for 40 min (G) and holding for 2 h followed by cooling from 1 369–300 °C at 900 °C/h for 1 h 11 min (H) and holding for 1 min, cooling from 300 °C to 80 °C at 900 °C/h for 15 min and holding for 15 min before final cooling from 80 °C to room temperature.

2.2. Surface morphology characterization

Field-emission scanning electron microscope (FE-SEM, Hitachi S-4800, JP) and electron dispersive spectroscopical (EDS) techniques were utilized for surface morphology studies and elemental identification, respectively. The EDS was used to produce spectral micrographs of selected spots on the specimens with individual elements identified from the spectral micrographs. Fig. 3 shows SEM images of both textured and

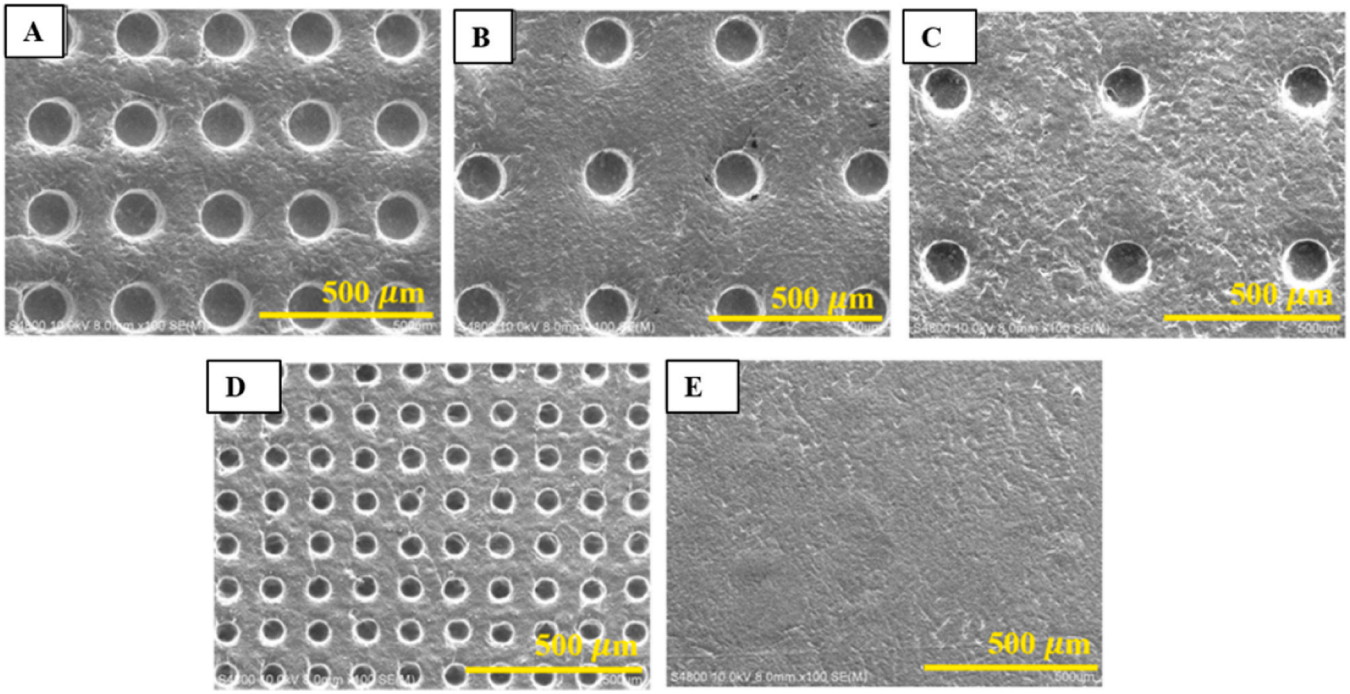

Fig. 3. SEM images of the fabricated WC-Co MIM micropit specimens before tribological tests. (A) 200 μm high density, (B) 400 μm medium density, (C) 600 μm low density, (D) 100 μm high density and (E) flat reference specimens at different magnifications.

flat WC-Co specimens before tribological tests.

Table 3 summarizes the geometries of the fabricated micropit and micropillar WC-Co specimens. It is noteworthy that the micropit specimens have smaller dimensions than micropillar specimens due to shrinkage of the 17-4PH SS during sintering of the SS mold.

2.3. Tribological testing

Reciprocating pin-on-plate sliding friction and wear tests were performed on both WC-Co specimens with micropits and flat reference WC-Co specimens against WC-Co pins (radius of curvature of 2.2 mm and length of 9.2 mm) using the CSM tribometer coupled with a computer controlled software. Tests were carried out in lubricated conditions using a commercial lubricating grease (SuperLube, Synco Chemicals, US) in combination with MoS_2 at different addition levels up to 50 wt%. MoS_2 was mixed together with SuperLube manually by simply adding the weighted percentage masses together in a small plastic tray, and a uniform mixture was obtained by gradual stirring. All lubricant mixtures were applied by rubbing 0.01 ml of lubricant unto the sliding track before sliding wear. Dispensing of lubricants onto the specimen surface was carried out using a 1 ml rubber syringe with a needle fitted at the tip. Two applied normal loads of 10 N and 30 N were employed. Each test was carried out at a linear acquisition rate of 100 Hz with a sliding distance of 100 m, sliding speed of 5 mm/s and an half amplidude of 15.0 mm. Temperature and humidity varied between the range of 25 ± 2 °C and 40 ± 2%, respectively at a standard atmospheric pressure. Test specimens were cleaned manually using acetone and cotton wool. Each test was repeated at least three times to enhance the reproducibilty and reliability of the obtained results.

3. Results and discussion

EDS spectral images of selected spots on the WC-Co sample specimens identified the highest peak in the measured spectrum as tungsten followed by the cobalt binder phase. The EDS analysis confirmed the presence of the main constituent elements; tungsten, carbon and cobalt in WC-Co, which constitute the two distinct phases, WC phase and Co phase of cemented tungsten carbides.

3.1. Optimization of MoS_2 additive level for sliding friction

Flat reference specimens were used to optimize the MoS_2 content in the lubricant. The measured dynamic COF values under an applied normal load of 10 N with different MoS_2 weight percentages are presented in Fig. 4. MoS_2 was mixed uniformly with the lubricating grease.

From Fig. 4, a gradual decrease in the dynamic COF curves from 0.11 for pure SuperLube is observed as the MoS_2 content increases. At 40 wt %, the curvature almost overlaps with the 50 wt% curve with 0.06 COF value. However, 50 wt% COF curvature begins to rise above the 40 wt% MoS_2 COF at the steady state after about 70 m of sliding distance. Therefore, 40 wt% was selected as the used amount in the following measurements with microstructured specimens.

3.2. Effect of micropit density at 40 wt% MoS_2 additive level

Fig. 5 shows the COF curves under two distinct applied normal loads, 10 N in A) and 30 N in B) with 40 wt% MoS_2. The dynamic COF curves

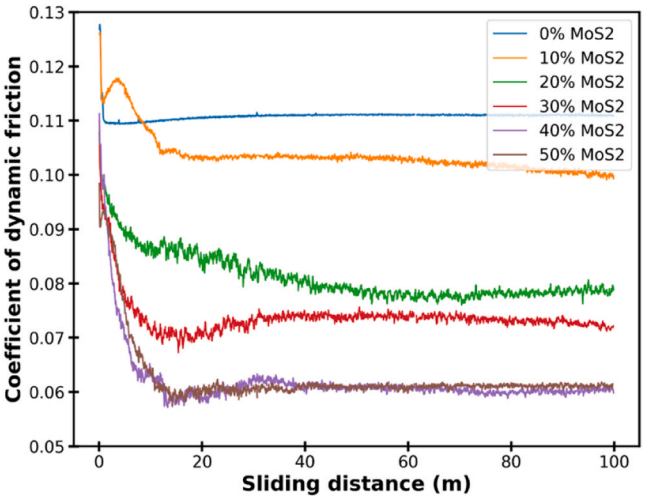

Fig. 4. COF curves for the flat reference specimens at varying MoS_2 levels.

for both textured and flat reference specimens are well below 0.10. It was observed that both medium and low density micropit specimens exhibited an irregular behavior. At 10 N, the low density micropit specimens present a lower dynamic COF value of 0.08 than the medium density specimens with 0.09 value, whereas at 30 N, the medium density specimens have a lower dynamic COF value of 0.08 compared to 0.10 for low density specimens.

The observed higher COF values for the micropit specimens compared to the flat WC-Co samples may also be related to relatively high viscosity of the used mixed lubricant. However, additional measurements with solid lubricants of paraffin wax mixed with MoS_2 showed that upon heating to a liquid form, these mixed waxes also displayed a similar COF behavior to SuperLube+MoS_2 lubricant although having a much higher viscosity. This indicated that the defining factor for the observed higher COF values for micropit specimens is not the high viscosity but rather the used pin getting bound to the edges of micropits.

As a summary, a rather regular behavior was observed both for the flat reference and the high density micropit specimens with steady state dynamic COF values of approximately 0.06 and 0.07, respectively, independent of the applied load. A previous study [30] reported a slight decrease in dynamic COF values but a significant increase in wear with increased applied normal load with WC-Co/WC-Co tribopairs but these tests were carried out under dry reciprocating sliding conditions.

3.3. Effect of micropit size on friction

The effect of micropit size on dynamic COF values was carried out using reciprocating sliding tests on WC-Co specimens having 100 μm size micropits with 100 μm separation between the adjacent pits. Each test was performed using 40 wt% MoS_2 at 10 N and 30 N applied normal loads as shown in Fig. 6. It is evident from Fig. 6A) that at a lower normal load of 10 N, the dynamic COF value was moderately low at 0.10 COF value and significantly lower than the corresponding value of 0.28 at 30 N shown in Fig. 6B). It can be concluded that decreasing the size of the micropit did not have a significant positive effect on the dynamic

Table 3
Final geometries of WC-Co micropit and micropillar specimens after sintering.

Micropits				Micropillars			
Matrices / (μm)	Top diameter/ (μm)	Bottom diameter/ (μm)	Depths/ (μm)	Matrices/ (μm)	Top diameter/ (μm)	Bottom diameter/ (μm)	Heights/ (μm)
200	143	126	42	200	162	195	55
400	141	123	52	400	167	193	43
600	140	128	35				

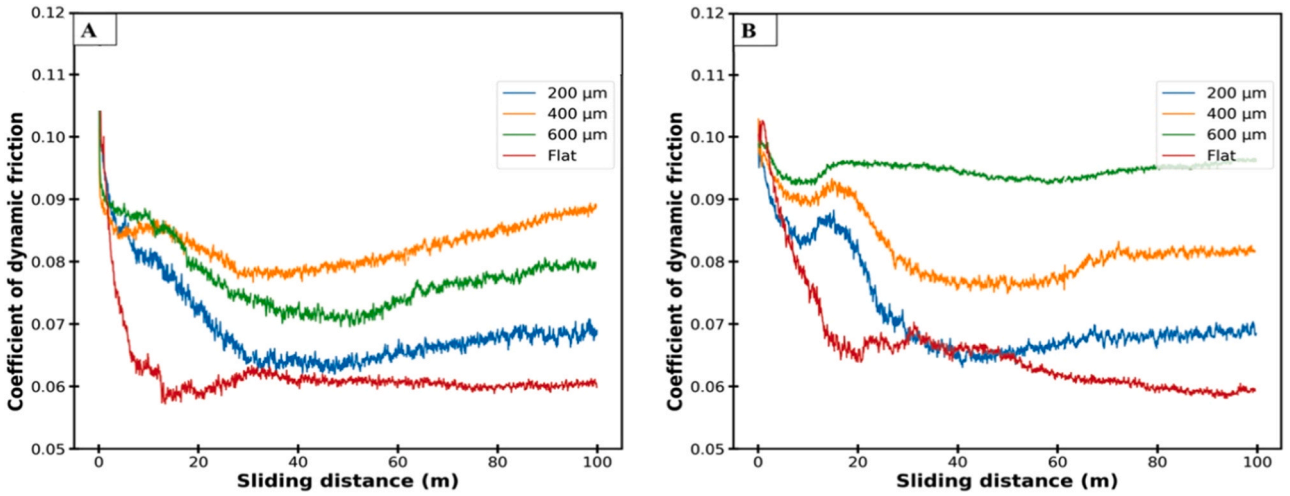

Fig. 5. COF curves for textured WC-Co specimens and flat WC-Co reference specimens at two distinct applied normal loads: (A) 10 N and (B) 30 N with 40 wt % MoS_2.

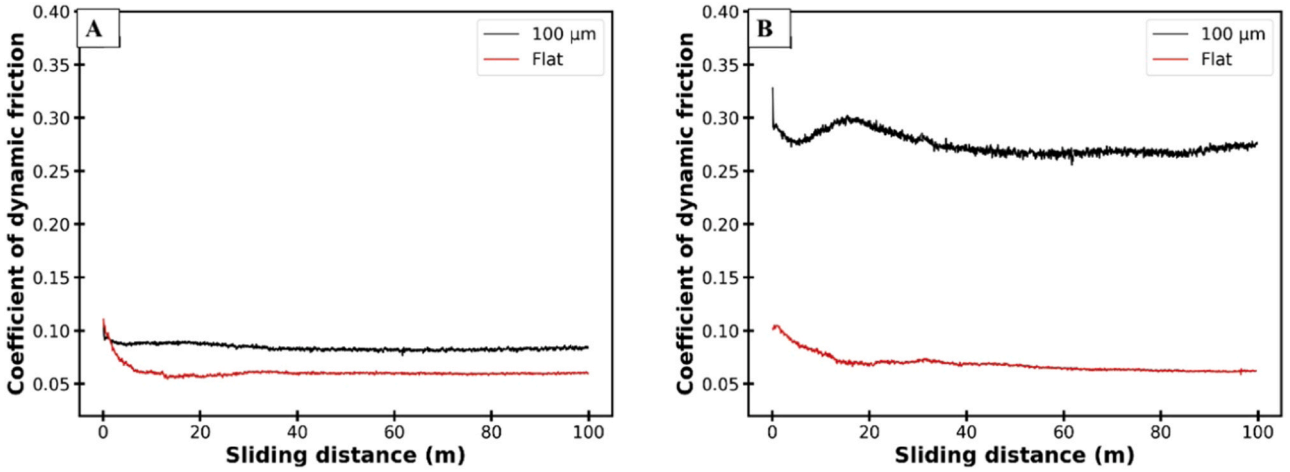

Fig. 6. Variation of COF curves at (A) 10 N and (B) 30 N for 100 μm micropit WC-Co specimens compared to the flat WC-Co reference specimens with 40 wt% MoS_2.

COF values. In a previous study [31] micropits or micro-dimples were observed to exhibit the lowest dynamic COF between rubbing surfaces when the dimple size was increased.

3.4. *Effect of micropillars on friction*

The effect of micropillars on dynamic COF values was studied with

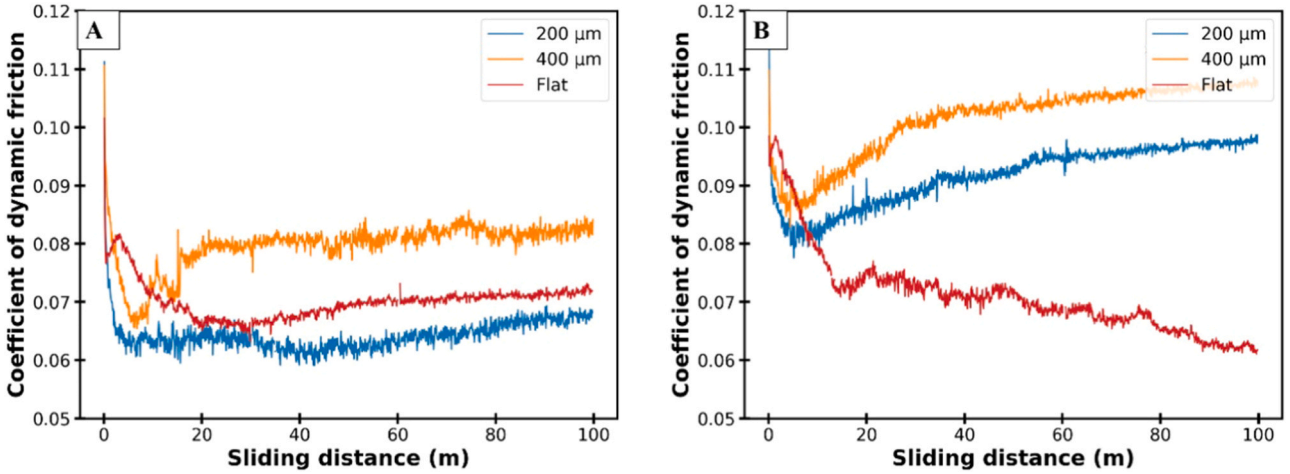

Fig. 7. COF curves for textured WC-Co micropillar specimens and flat WC-Co reference specimens at a half amplitude of 20 mm with 40 wt% MoS_2 at (A) 10 N and (B) 30 N.

comparative reciprocating sliding tests that were run on selected WC-Co test specimens. 200 μm high density and 400 μm low density micropillar specimens with flat specimens were measured with lubricating grease mixed with 40 wt% MoS_2 at 10 N and 30 N as shown in Fig. 7. Here the sliding tests were carried out using a half amplitude of 20 mm as the structured area was larger compared to the micropit specimens, whereas all other test parameters were similar to the micropit specimens. In Fig. 7A), at 10 N applied normal load the 200 μm high density specimens showed a lower COF value of 0.06 than the flat reference specimens with 0.08 and the 400 μm low density specimens with 0.09. On the contrary, as the applied normal load was increased to 30 N in Fig. 7B), dynamic COF values decreased steadily for the flat reference specimens of 0.07, whereas the COF values of the micropillar specimens were higher at approximately 0.1. It can be concluded that in this case the high density micropillar specimen exhibited a lower COF value at 10 N normal load than the flat reference specimens.

3.5. Surface analysis after the wear

The wear mechanisms on the surfaces of test specimens was studied from the SEM images after tribological testing. The surfaces were cleaned using acetone and cotton wool before the SEM imaging. All tribological tests were carried out under normal loads of 10 N and 30 N that did not result in a significant wear on the surfaces.

Fig. 8 A - D) shows SEM images of the high, medium, and low density micropits with a flat reference specimen after sliding friction and wear test at a 10 N normal load with 40 wt% MoS_2 content. Sheet-like fragments of the mixed lubricants are entrapped within the micropits Fig. 8A). However, no observable wear tracks were visible on the worn surfaces excluding a narrow-polished wear track on the flat reference specimens Fig. 8D and H).

Fig. 8E - H) shows the corresponding specimens after tribological tests under 30 N applied normal load. Similar to the observations at 10 N normal load presented in Fig. 8A), the wear tracks were barely noticeable on the worn surfaces, excluding the flat reference specimens with a clear worn area. On the contrary, only fragmented plate-like sheets of the mixed lubricants were visibly entrapped within the micropits Fig. 8E).

Fig. 9 presents the SEM images of the micropillar specimens with a flat reference specimen at normal load of 10 N (Fig. 9A - C) and 30 N (Fig. 9D - F). It is clear from the SEM images that wear increases with an increasing normal load [30], especially for the micropillar specimens that display severely ploughed and broken micropillar structures along the top and edges. However, only moderate wear mechanism was observed on top of the low density micropillars at 10 N. Surface polishing was also observed on the flat reference specimen Fig. 9C) at 10 N with a narrow, weak wear track compared to the worn track Fig. 9F) at 30 N normal load.

As a summary, the flat reference specimen displayed the lowest dynamic COF values. Hence, surface texturing did not have significant benefit over the flat specimens in terms of the dynamic COF values, with the exception of the 200 μm high density micropillar specimens. However, as reported in a previous study [32], micro-dimples on specimen surfaces can have both postive and negative effects on the dynamic COF. The dimples can serve as reservoir space for lubricant and entrapping wear debris that can reserve lubrication between tribopairs. This may help in formation of a lubricating film between the rubbing surfaces compared to a flat reference surface i.e. a dimple specimen can sustain a reduced friction at the interface for a longer duration of a wearing action. On the contrary, dimple structure can also present a negative effect of increasing surface contact pressure due to reduction in the real contact area. Thus, controlling friction between rubbing surfaces under the combined influence of both surface microstructure and lubrication depends on which of these two opposite effects of the dimples prevails under the selected test conditions [32].

It can be concluded that in this study the interface contact pressure on the textured surfaces was higher than the positive influence of micropits trapping and supplying lubricants onto the sliding surface. This is probably due to the small contact area of the used spherical tips of the pins. In the case of specimens with micropillars, the 200 μm high density specimens displayed a lower COF value than the flat reference specimen. This is probably due to the support of micro-structures improving the load carrying capacity of the specimens. To increase the surface contact area, a flat headed pin was also tested. Unfortunately, this resulted in a very non-uniform contact with test specimens and alignment problems between the tip and the sample that are not present with spherical tips. Therefore, high variations in the measured data were observed. Increasing the radius of curvature of the tip could reduce the tip penetration depth into the microstructure that would result in a lower COF values. We plan to return to this issue in a future communication.

It can also be concluded that under the selected test conditions, wear resistance performance of the test specimens was remarkable. Only mild wear in the form of surface polishing was observed on the specimen sufaces after tribological testing, which suggests plastic deformation of surface during sliding [32]. However, as compared to the specimens

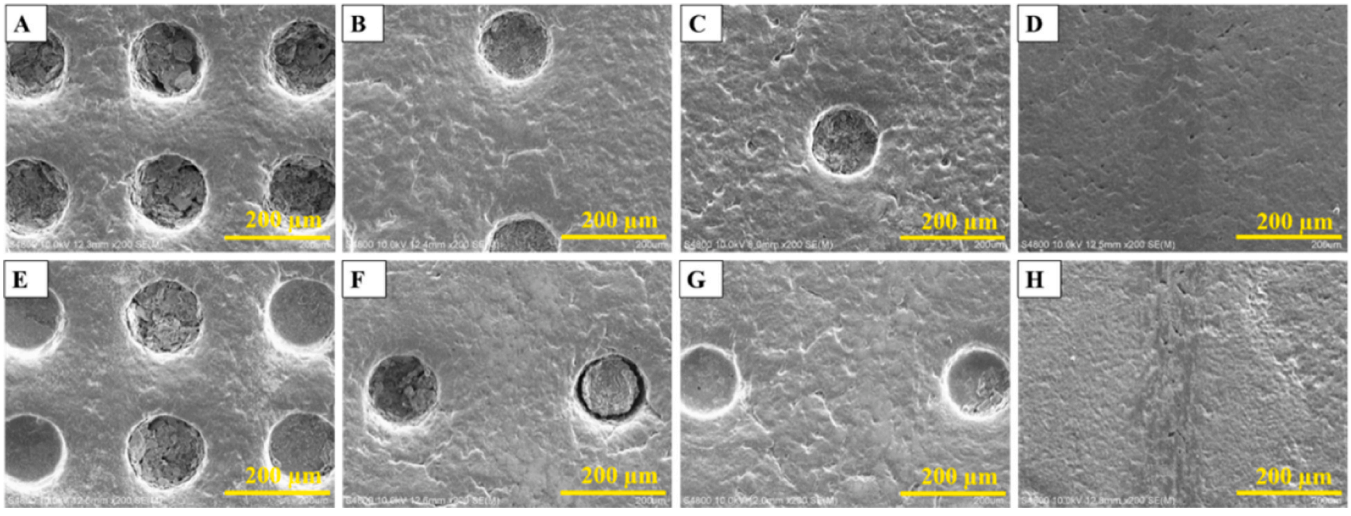

Fig. 8. SEM images of worn micropit surfaces after tribological test with 40 wt% MoS_2 at 10 N (A - D) and 30 N (E - H) applied normal load. (A and E) 200 μm high density, (B and F) 400 μm medium density, (C and G) 600 μm low density micropit specimens and (D and H) flat reference specimens.

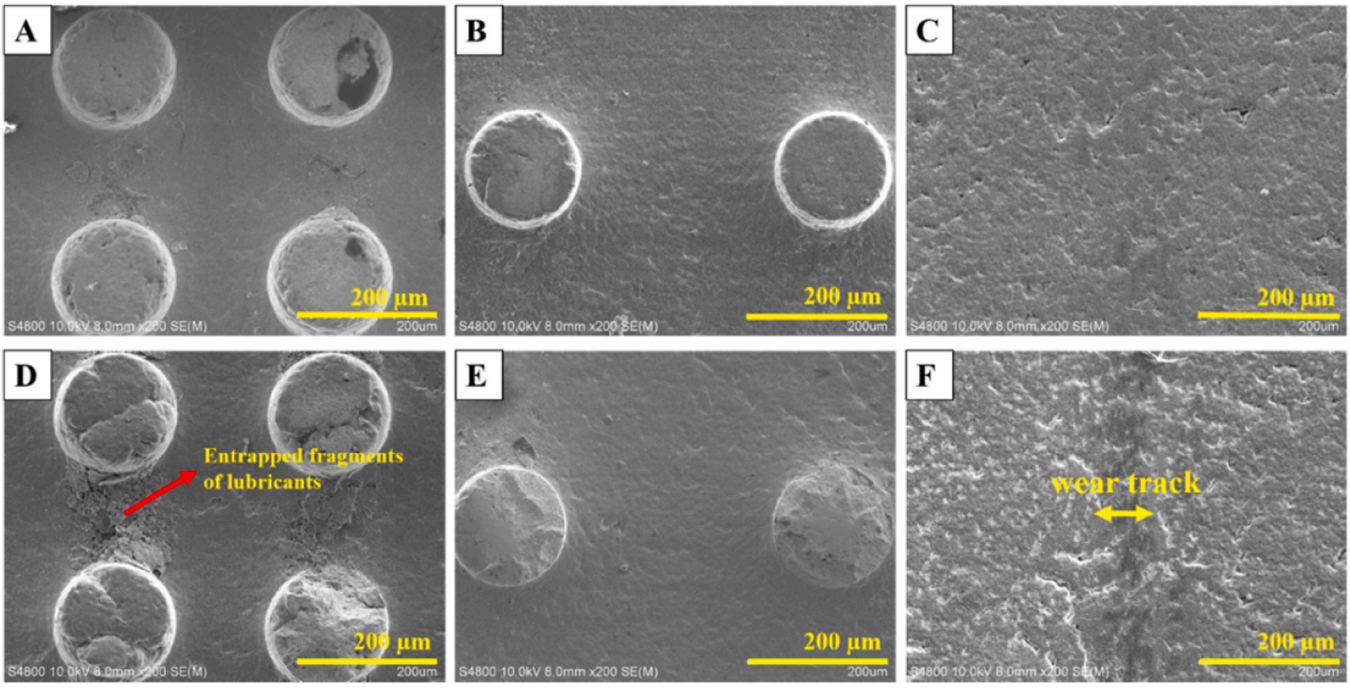

Fig. 9. SEM images of micropillar specimens after tribological test with 40 wt% MoS_2 at 10 N (A-C) and 30 N (D-F) normal load. (A and D) 200 µm high density, (B and E) 400 µm low density and (C and F) flat reference specimens.

with micropillars, the specimens with micropits exhibited a better antiwear behavior at both used normal loads in this study.

4. Conclusions

Highly ordered round shaped micropits and micropillars with variable sizes were manufactured on WC-Co hard metals specimens using micro-robot and MIM techniques. The influence of a solid lubricant (MoS_2) addition to lubricating grease on the tribological performance was investigated. The best weighted percentage amount of MoS_2 was observed at 40 wt%, among those tested, which presented good synergy with lubricating grease both in terms of friction coefficient and wear performance. COF values well below 0.100 were recorded with the flat reference specimenS and the 200 µm size high density micropit specimens that exhibited the best tribological behavior. For the micropillar specimens, the 200 µm high density specimens presented a lower COF value compared to the flat reference specimen.

For the micropit specimens, lower COF values were obtained with increased size and density of micropits. Hence, the 200 µm size high density micropit specimens performed better than 100 µm micropits specimens. However, the micropits played the significant role of entrapping wear debris and retaining the lubricants on the specimen surface. The tribopairs were highly stable under the test conditions, and highly stable antiwear behavior was observed on all test specimens.

CRediT authorship contribution statement

Christopher K. Dawari: investigation, writing – original draft. **Inzimam Haq**: investigation. **Kari Mönkkönen**: conceptualization, funding acquisition, project administration, resources. **Mika Suvanto**: conceptualization, funding acquisition, project administration, resources, supervision, writing – review & editing. **Jarkko J. Saarinen**: conceptualization, project administration, supervision, writing – review & editing.

Declaration of Competing Interest

The authors declare that they have no known competing financial interests or personal relationships that could have appeared to influence the work reported in this paper.

Acknowledgments

We gratefully acknowledge the Business Finland/ERDF (European Regional Development Fund) project "MIM Components for Harsh Conditions" (Grant agreement 7929/31/2019) for financial support. J.J. S. acknowledges the Faculty of Science and Forestry at the University of Eastern Finland for financial support (grant no. 579/2017) and the Academy of Finland Flagship for Photonics Research and Innovation (PREIN, decision no. 320166).

References

[1] An V, Irtegov Y, De Izarra C. Study of tribological properties of nanolamellar WS_2 and MoS_2 as additives to lubricants. J Nanomater 2014;2014:1–8.
[2] Suarez MP, Marques A, Boing D, Amorim FL, Machado ÁR. MoS_2 solid lubricant application in turning of AISI D6 hardened steel with PCBN tools. J Manuf Process 2019;47:337–46.
[3] An V, Anisimov E, Druzyanova V, Burtsev N, Shulepov I, Khaskelberg M. Study of tribological behavior of Cu–MoS_2 and Ag–MoS_2 nanocomposite lubricants. Springerplus 2016;5(1):1–5.
[4] Yan C, Zeng Q, Hao Y, Xu Y, Zhou M. Friction-induced hardening behaviors and tribological properties of 60NiTi alloy lubricated by lithium grease containing nano-BN and MoS_2. Tribol Trans 2019;62(5):812–20.
[5] Rapoport L, Leshchinsky V, Lapsker I, Volovik Y, Nepomnyashchy O, Lvovsky M, Popovitz-Biro R, Feldman Y, Tenne R. Tribological properties of WS2 nanoparticles under mixed lubrication. Wear 2003;255(7–12):785–93.
[6] Rodriguez V, Sukumaran J, Schlarb AK, De Baets P. Influence of solid lubricants on tribological properties of polyetheretherketone (PEEK). Tribol Int 2016;103:45–57.
[7] Prajapati AK, Omrani E, Menezes PL, Rohatgi PK. Fundamentals of solid lubricants. Self-Lubricating Composites. Berlin Heidelberg: Springer; 2018. p. 1–32.
[8] Domínguez-Meister S, Rojas TC, Brizuela M, Sánchez-López JC. Solid lubricant behavior of MoS2 and WSe2-based nanocomposite coatings. Sci Technol Adv Mater 2017;18(1):122–33.
[9] Vazirisereshk MR, Martini A, Strubbe DA, Baykara MZ. Solid lubrication with MoS_2: a review. Lubricants 2019;7(7):57.
[10] Furlan KP, de Mello JDB, Klein AN. Self-lubricating composites containing MoS2: a review. Tribol Int 2018;120:280–98.

[11] Li Y, Xie M, Sun Q, Xu X, Fan X, Zhang G, Li H, Zhu M. The effect of atmosphere on the tribological behavior of magnetron sputtered MoS2 coatings. Surf Coat Technol 2019;378:125081.
[12] Zhang K, Deng J, Lei S, Yu X. Effect of micro/nano-textures and burnished MoS2 addition on the tribological properties of PVD TiAlN coatings against AISI 316 stainless steel. Surf Coat Technol 2016;291:382–95.
[13] Panin SV, Jiangkun L, Kornienko LA, Buslovich DG, Alexenko VO, Ivanova LR. Mechanical and tribotechnical properties of polyimide based solid lubricant composites. AIP Conf Proc 2019;2167(1):020266.
[14] Wu Z, Deng J, Zhang H, Lian Y, Zhao J. Tribological behavior of textured cemented carbide filled with solid lubricants in dry sliding with titanium alloys. Wear 2012; 292–293:135–43.
[15] Hu T, Hu L, Ding Q. Effective solution for the tribological problems of Ti-6Al-4V: combination of laser surface texturing and solid lubricant film. Surf Coat Technol 2012;206(24):5060–6.
[16] Rapoport L, Moshkovich A, Perfilyev V, Lapsker I, Halperin G, Itovich Y, Etsion I. Friction and wear of MoS_2 films on laser textured steel surfaces. Surf Coat Technol 2008;202(14):3332–40.
[17] Ananth MP, Ramesh R. Sliding wear characteristics of solid lubricant coating on titanium alloy surface modified by laser texturing and ternary hard coatings. Trans Nonferrous Metals Soc China 2017;27(4):839–47 (English Ed.).
[18] Hu T, Zhang Y, Hu L. Tribological investigation of MoS2 coatings deposited on the laser textured surface. Wear 2012;278–279:77–82.
[19] Zhang R, Cui Q, Weng L, Sun J, Hu M, Fu Y, Wang D, Jiang D, Gao X. Modification of structure and wear resistance of closed-field unbalanced-magnetron sputtered MoS2 film by vacuum-heat-treatment. Surf Coat Technol 2020;401:126215.
[20] Vaitkunaite G, Espejo C, Wang C, Thiébaut B, Charrin C, Neville A, Morina A. MoS_2 tribofilm distribution from low viscosity lubricants and its effect on friction. Tribol Int 2020;151:106531.
[21] Sgroi MF, Asti M, Gili F, Deorsola FA, Bensaid S, Fino D, Kraft G, Garcia I, Dassenoy F. Engine bench and road testing of an engine oil containing MoS2 particles as nano-additive for friction reduction. Tribol. Int. 2017;105:317–25.
[22] Liu L, Zhou W. MoS_2 hollow microspheres used as a green lubricating additive for liquid paraffin. Tribol Int 2017;114:315–21.
[23] Arslan A, Masjuki HH, Kalam MA, Varman M, Mufti RA, Mosarof MH, Khuong LS, Quazi MM. Surface texture manufacturing techniques and tribological effect of surface texturing on cutting tool performance: a review. Crit Rev Solid State Mater Sci 2016;41(6):447–81.
[24] Ammosova L, Mönkkönen K, Suvanto M. Precise fabrication of microtextured stainless steel surfaces using metal injection moulding. Precis Eng 2020;62:89–94.
[25] Li W, Zhang Z. Effect of cutting tool with micro-pits texture on wood cutting performance. PLoS One 2019;14(4):e0214888.
[26] Kovalchenko A, Ajayi O, Erdemir A, Fenske G. Friction and wear behavior of laser textured surface under lubricated initial point contact. Wear 2011;271(9–10): 1719–25.
[27] Zhang X, Qu N, Fang X. Sandwich-like electrochemical micromachining of micro-dimples using a porous metal cathode. Surf Coat Technol 2017;311:357–64.
[28] Shi L, Wang X, Su X, Huang W, Wang X. Comparison of the load-carrying performance of mechanical gas seals textured with microgrooves and microdimples. J Tribol 2016;138(2).
[29] Kligerman Y, Etsion I. Analysis of the hydrodynamic effects in a surface textured circumferential gas seal. Tribol Trans 2001;44(3):472–8.
[30] Bonny K, De Baets P, Perez Y, Vleugels J, Lauwers B. Friction and wear characteristics of WC-Co cemented carbides in dry reciprocating sliding contact. Wear 2010;268(11–12):1504–17.
[31] Wakuda M, Yamauchi Y, Kanzaki S, Yasuda Y. Effect of surface texturing on friction reduction between ceramic and steel materials under lubricated sliding contact. Wear 2003;254(3–4):356–63.
[32] Uehara Y, Wakuda M, Yamauchi Y, Kanzaki S, Sakaguchi S. Tribological properties of dimpled silicon nitride under oil lubrication. J. Eur. Ceram. Soc. 2004;24(2): 369–73.